



A Journal of the Gesellschaft Deutscher Chemiker

Angewandte Chemie

GDCh

International Edition

www.angewandte.org

Accepted Article

Title: Fe-Co Alloyed Nanoparticles Catalysed Efficient Hydrogenation of Cinnamaldehyde to Cinnamyl Alcohol in Water

Authors: Yang Lv, Miaomiao Han, Wanbing Gong, Dongdong Wang, Chun Chen, Guozhong Wang, Haimin Zhang, and Huijun Zhao

This manuscript has been accepted after peer review and appears as an Accepted Article online prior to editing, proofing, and formal publication of the final Version of Record (VoR). This work is currently citable by using the Digital Object Identifier (DOI) given below. The VoR will be published online in Early View as soon as possible and may be different to this Accepted Article as a result of editing. Readers should obtain the VoR from the journal website shown below when it is published to ensure accuracy of information. The authors are responsible for the content of this Accepted Article.

To be cited as: *Angew. Chem. Int. Ed.* 10.1002/anie.202009913

Link to VoR: <https://doi.org/10.1002/anie.202009913>

Fe-Co Alloyed Nanoparticles Catalysed Efficient Hydrogenation of Cinnamaldehyde to Cinnamyl Alcohol in Water

Yang Lv,^{+[a,b]} Miaomiao Han,^{+[a]} Wanbing Gong,^{+[a]} Dongdong Wang,^[a,b] Chun Chen,^[a] Guozhong Wang,^[a] Haimin Zhang^[a] and Huijun Zhao^{+[a,c]}

Abstract: Selective hydrogenation of C=O against the conjugated C=C in cinnamaldehyde (CAL) is indispensable to produce cinnamyl alcohol (COL), nonetheless, challenged by the low selectivity and the need to use organic solvents. Herein, for the first time, we report the use of Fe-Co alloy nanoparticles (NPs) on N-doped carbon support as a selective hydrogenation catalyst to efficiently convert CAL to COL. The resultant catalyst with the optimized Fe/Co ratio of 0.5 can achieve an exceptional COL selectivity of 91.7% at a CAL conversion of 95.1% in pure water medium under mild reaction conditions, ranking it the best performed catalyst reported to date. The experimental results confirm that the COL selectivity and CAL conversion efficiency are respectively promoted by the presence of Fe and Co, while the synergism of the alloyed Fe-Co is the key to concurrently achieve high COL selectivity and CAL conversion efficiency.

Cinnamyl alcohol (COL) is an essential substance/precursor highly demanded by flavouring, perfume and pharmaceutical industries.^[1-4] To date, the industrial production of COL has been carried out exclusively *via* the selective hydrogenation (SH) of cinnamaldehyde (CAL) in organic solvents.^[5-7] The efficiently utilizing CAL is the most critical issue for COL production because large quantities of CAL can only be obtained in an economically viable manner *via* extraction processes from the bark of cinnamon and other CAL containing trees with limited nature reserves. Presently, SH of CAL to COL is challenged by the unfavoured thermodynamics that leads to low selectivity toward COL.^[1,8-10] Also, the use of organic solvent in COL production pollutes the environment and requires post-production separation. For these reasons, the relevant industries

have constantly demanded to replace organic solvents with water, however, the development of new catalysts capable of SH of CAL in pure aqueous medium is required.

To improve the selectivity towards COL, various strategies have been reported. One widely investigated strategy is to create a steric hindrance barrier on the catalyst surface *via* chelating organic ligands^[9,11,12] or encapsulating the catalytic active sites by metal-organic frameworks (MOFs)^[1,5,13] that regulates the spatial orientation of CAL to facilitate CAL approaching the catalytic active sites with its C=O group. Nonetheless, the enhanced COL selectivity is accompanied by the reduced CAL conversion efficiency due to the suppressed mass transport by the selectivity barriers.^[1,9] Another strategy employs transition-metal/noble-metal (Pt is the most used) bimetallic catalysts to create synergetic electronic effects that thermodynamically favoured the hydrogenation of C=O in CAL.^[6,14-16] In theory, this strategy can enhance COL selectivity without compromising the CAL conversion efficiency, however, the use of scarce and expensive noble-metals is undesirable.

Up till now, only few literatures reported the use of water as the solvent and nonprecious metals as the catalyst for SH of CAL.^[11,17] For example, Ni₂P innovatively chelated with *p*-fluorothiophenol was reported by Zou's group to create steric and electronic effects for SH of CAL in both aqueous and organic solvents.^[11] They successfully demonstrated a high COL selectivity of 91.2%, but with a reduced CAL conversion to 40.2%, due to the chelating layer induced mass transport resistance. Another example employed a copper cluster encapsulated by a dendrimer selectivity barrier for hydrogenation of a series of substrates including CAL. The catalyst is capable of SH of CAL to produce COL in water with excellent selectivity and conversion efficiency, nonetheless, requiring to use a large amount of NaBH₄ after each catalytic run to regenerate the oxidized catalyst.^[17] Recently, Yang's group reported the first systematic mechanistic investigation of SH of CAL to COL at carbon nanotube (CNT) supported bimetallic PtFe catalysts in pure water.^[6] Their theoretic studies and the experimental results revealed a direct water participation hydrogen-exchange pathway that can dramatically reduce the energy barrier of hydrogenation of C=O in CAL. The best performed catalyst (Pt₃Fe/CNT) can achieve a high COL selectivity of 97.2% with a CAL conversion of 62.1%. Despite the enormous efforts and noticeable progress, the highly efficient nonprecious catalyst for SH of CAL to COL in pure water has yet been developed.

Herein, we report a bimetallic transition-metals alloying strategy to realise highly efficient conversion of CAL to COL in pure water medium. A solution-based metal ion impregnation approach is innovatively combined with pyrolysis to achieve the controllable synthesis of highly dispersed Fe-Co alloy

[a] Y. Lv⁺, Dr. M. Han⁺, Dr. W. Gong, D. Wang, Dr. C. Chen, Prof. G. Wang, H. Zhang, H. Zhao
Key Laboratory of Materials Physics
Centre for Environmental and Energy Nanomaterials
Anhui Key Laboratory of Nanomaterials and Nanotechnology
CAS Centre for Excellence in Nanoscience, Institute of Solid State Physics, Chinese Academy of Sciences
Hefei 230031, (P. R. China)
Tel: (+86) 551 65591263
E-mail: h.zhao@griffith.edu.au, wbgong@issp.ac.cn

[b] Y. Lv⁺, D. Wang,
University of Science and Technology of China
Hefei 230026, P. R. China

[c] Prof. H. Zhao
Centre for Clean Environment and Energy
Gold Coast Campus
Griffith University
Queensland 4222, Australia

[+] These authors contributed equally to this work

Supporting Information for this article is available on the WWW under

nanoparticles (NPs) on N-doped graphitic carbon support. The Fe-Co alloy catalyst with an optimal Fe/Co molar ratio of 0.5 can concurrently achieve an exceptional COL selectivity of 91.7% at a CAL conversion of 95.1%, ranking it the best performed catalyst reported to date.

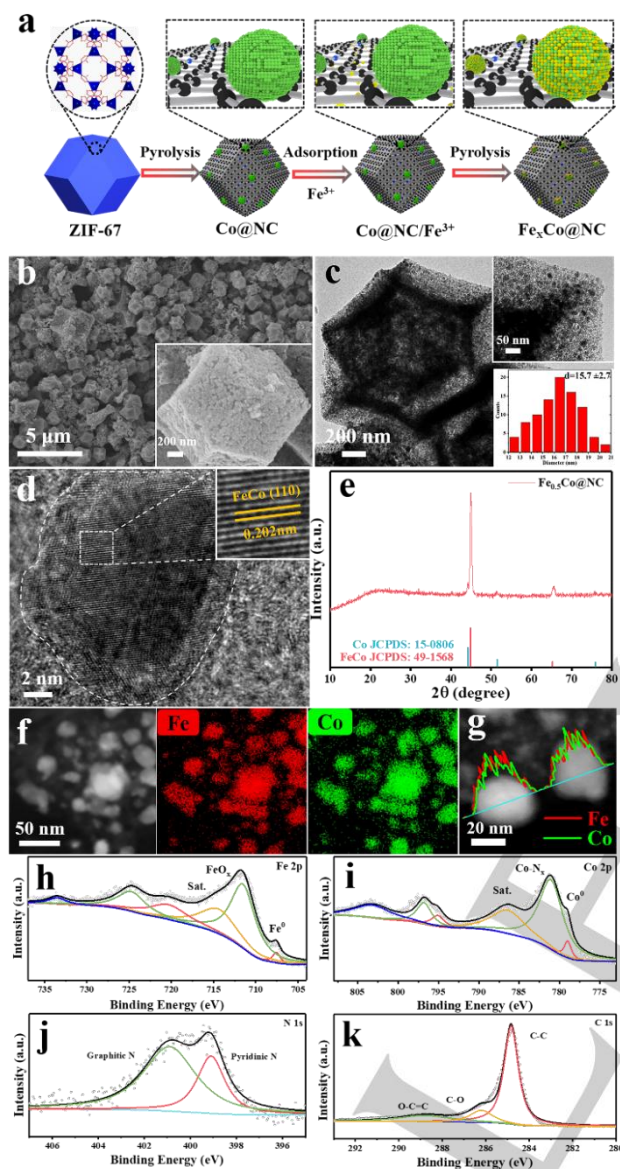


Figure 1. (a) Schematic illustration of synthetic procedure of $\text{Fe}_x\text{Co@NC}$; (b-c) SEM (inset: high-magnification SEM image) and TEM (insets: high-magnification TEM image and Fe-Co NPs size distribution) images; (d) HRTEM image (inset: high-magnification HRTEM image) of a Fe-Co NP; (e) XRD pattern; (f-g) HAADF-STEM, corresponding elemental mapping images and line profile of Fe-Co NPs; (h-k) High resolution XPS spectra of Fe 2p, Co 2p, N 1s and C 1s of $\text{Fe}_{0.5}\text{Co@NC}$.

Figure 1a schematically illustrates the synthetic procedure of Fe-Co alloy NPs on N-doped graphitic carbon support (denoted as $\text{Fe}_x\text{Co@NC}$, where, X represents the Fe/Co molar ratio). In brief, the synthesised rhombic dodecahedron-shaped ZIF-67 crystals^[18-20] with sized between 1-2 μm (Figure S1) were used as the precursor and firstly subjected to carbonization treatment under H_2/Ar atmosphere. The carbonized product (denoted as Co@NC) retains the rhombic dodecahedron-shape with densely populated Co NPs having an average size of 12.1 nm (Figures S2-3).^[18,19] The inductively coupled plasma (ICP)

analysis indicates a 46.8 wt.% cobalt content in the obtained Co@NC (Table S1). The resultant Co@NC was dispersed in n-hexane, and the aqueous solution containing Fe^{3+} was added drop-wisely under ultrasonication to achieve Fe^{3+} impregnation.^[21,22] The resultant Co@NC with impregnated Fe^{3+} (denoted as Co@NC/Fe^{3+}) was then thermally treated under a reductive H_2/Ar atmosphere to obtain $\text{Fe}_{0.5}\text{Co@NC}$. The ICP analysis confirm the presence of 17.9 wt.% and 37.1 wt.% of Fe and Co, respectively, equivalent to a Fe/Co molar ratio of 0.51 (Table S1). Typical scanning electron microscopy (SEM) images (Figure 1b) reveal that the size and shape of the obtained $\text{Fe}_{0.5}\text{Co@NC}$ are similar to that of Co@NC . Transmission electron microscopic (TEM) images (Figure 1c) confirm that the metallic NPs with an average size of 15.7 nm are homogeneously embedded on the carbon support. The high-resolution TEM (HRTEM) images of a typical NP (Figure 1d) display a d-spacing of 0.202 nm, corresponding to the {110} faceted metallic Fe-Co alloy. The X-ray diffraction (XRD) pattern (Figure 1e) shows two peaks centred at 44.9° and 65.3° , which are the signature diffraction peaks of the (110)/(200) faceted Fe-Co alloy phase (JCPDS No. 49-1568). The high-angle annular dark-field scanning transmission electron microscopy (HAADF-STEM) and the corresponding elemental mapping images (Figure 1f) confirm that Fe and Co are homogeneously distributed in the Fe-Co alloy NPs. The line profiles of representative NPs (Figure 1g) further confirm the homogeneously distributed Fe and Co in the alloyed NPs. The survey X-ray photoelectron spectroscopy (XPS) spectrum of $\text{Fe}_{0.5}\text{Co@NC}$ indicates the presence of Fe, Co, C and N (Figure S4). The high resolution Fe 2p spectrum (Figure 1h) indicates the presence of metallic (707.4 and 720.1 eV) and ionic (711.3 and 724.7 eV) forms of Fe, while the peaks centred at 714.4 and 733.5 eV can be attributed to the shakeup satellite peaks.^[23-25] The high resolution Co 2p spectrum (Figure 1i) indicates the presence of Co^0 (779.0 and 794.1 eV),^[23,26] while the peaks centred at 781.1 and 796.8 eV with shakeup satellites (786.4 and 803.2 eV) correspond to Co-N_x species.^[19,26,27] The high resolution N 1s (Figure 1j) and C 1s (Figure 1k) spectra reveal the existence of pyridinic N (398.9 eV) and graphitic N (400.9 eV),^[28,29] and sp^2 -hybridized carbon (284.8 eV), C-O bonds (286.5 eV) and O-C=O group (288.8 eV).^[26,30]

As shown in **Figure 2**, the SH of CAL could occur at C=O or C=C or both, leading to the formation of COL or hydrocinnamaldehyde (HCAL) or hydrocinnamyl alcohol (HCOL), respectively. The catalytic performance of $\text{Fe}_{0.5}\text{Co@NC}$ was evaluated. The effect of reaction temperature was firstly investigated under 2 MPa H_2 pressure for 2 h (Figure 2a). The CAL conversion is found to increase from 34.2 to 99.1% as the temperature increasing from 50 to 100 $^\circ\text{C}$. Within 50-80 $^\circ\text{C}$, the COL selectivity decreased slightly from 93.1 to 91.7%, which suggest that $\text{Fe}_{0.5}\text{Co@NC}$ catalysed hydrogenation on C=O is more favourable than that of C=C under relatively low temperatures. Interestingly, beyond 80 $^\circ\text{C}$, the COL selectivity decreased rapidly to 24.6%, accompanying by the rapidly increased HCOL selectivity from 5.5 to 73.0%. These indicate that the rapidly decreased COL selectivity at higher temperatures is due to the occurrence of hydrogenation on both C=O and C=C.^[31] The effect of reaction time was then evaluated under 2 MPa H_2 pressure and 80 $^\circ\text{C}$. As revealed in Figure 2b, an increase in the reaction time from 0.5 to 2 h leads to a rapid

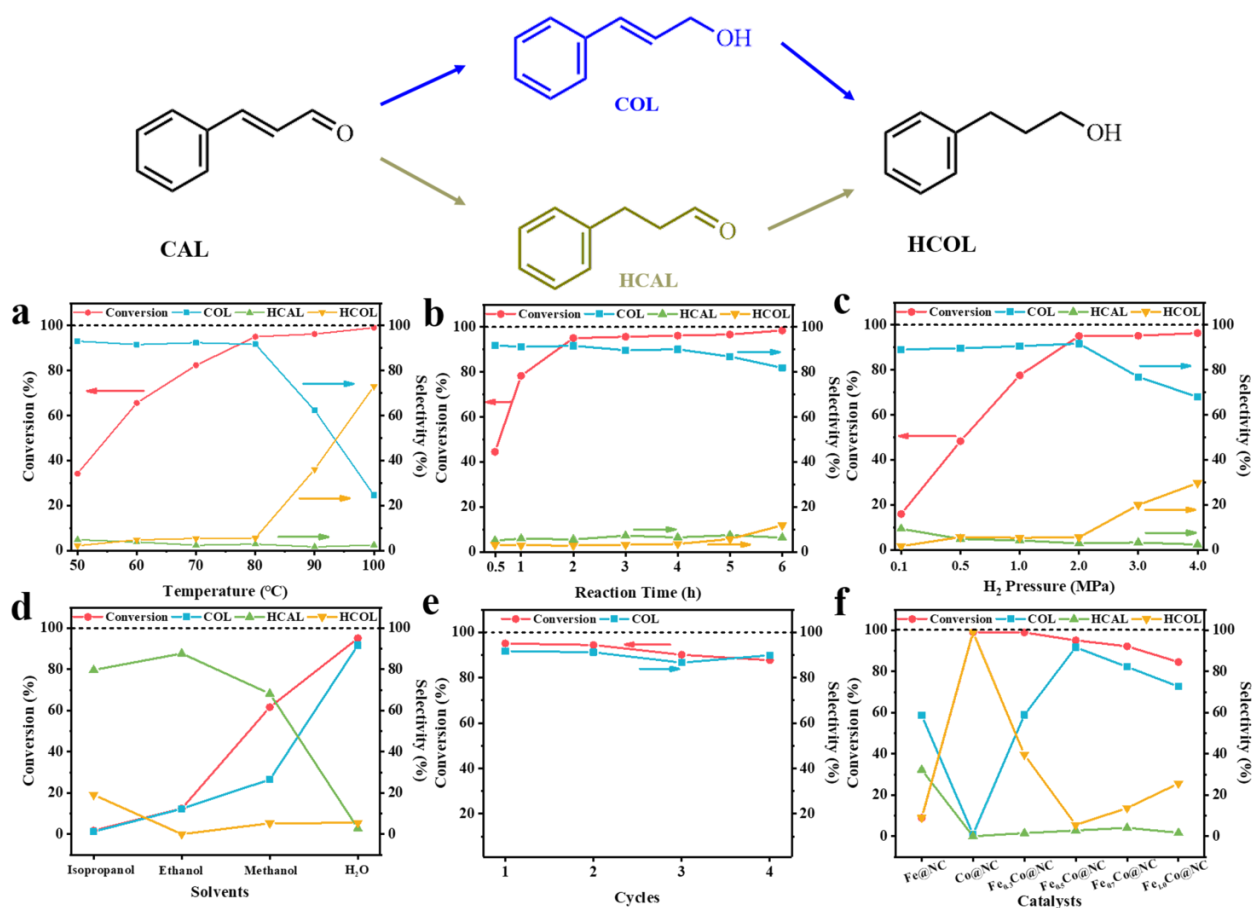


Figure 2. Effect of (a) reaction temperature (2 h, 2 MPa H₂, H₂O); (b) reaction time (80 °C, 2 MPa H₂, H₂O); (c) H₂ pressure (80 °C, 2 h, H₂O) and (d) solvent (80 °C, 2 MPa H₂, 2 h) on CAL conversion efficiency and COL selectivity of Fe_{0.5}Co@NC catalysed SH of CAL to COL. (e) Reusability of Fe_{0.5}Co@NC (80 °C, 2 MPa H₂, 2 h, H₂O). (f) Catalytic performance of Fe@NC, Co@NC and Fe_xCo@NC (80 °C, 2 MPa H₂, 2 h, H₂O). Catalyst: 20 mg; CAL: 1 mmol; Solvent: 10 mL.

increase in CAL conversion from 44.5 to 95.1% and further increase in the reaction time results in a neglectable increase in CAL conversion. In contrast, the COL selectivity remained at 91.7% before decreased to 81.9% at 6 h due to the increased HCOL selectivity beyond 5 h. The dependent on H₂ pressure was investigated at 80 °C with 2 h reaction time (Figure 2c). An increase in H₂ pressure to 2 MPa leads to a linearly increased CAL conversion to 95.1% and levelled off with further increased H₂ pressures. As expected, within a 2 MPa H₂ pressure range, the COL selectivity increased slightly from 89.1 to 91.7%, then linearly decreased to 68.0% with further increased H₂ pressure to 4 MPa due to the increased hydrogenation on both C=O and C=C to form HCOL. In addition, the catalyst performance in different solvents was studied (Figure 2d). The CAL conversion efficiencies follow a trend of H₂O (95.1%) > methanol (61.6%) > ethanol (12.4%) > isopropanol (1.7%). This indicates that the higher the solvent polarity, the higher the CAL conversion efficiency. Such correlations between the solvent polarity and CAL conversion efficiency was also observed by other studies.^[32,33] Another reason could be that N species enhance the hydrophilicity of carbon-based catalysts, which is beneficial for CAL approaching the surface of catalyst.^[34,35] Although the selectivity toward COL follows the same solvent polarity trend, the generation of the by-products cannot be directly correlated to the polarity of solvents. Nevertheless, the promotional effect of H₂O solvent to remarkably enhance the hydrogenation on C=O and concurrently suppress the hydrogenation on C=C is categorically confirmed. This is likely due to the strong

interactions/possible hydrogen-bond formations of H₂O with C=O and catalyst surface site that makes the selective adsorption of CAL on catalyst surface site *via* C=O a preference hydrogenation reaction step, leading to an accelerated reaction kinetics and improved COL selectivity.^[6] The achieved performance of Fe_{0.5}Co@NC under these conditions is the best among the reported high performance catalysts for SH of CAL in water (Tables S2 and 3). Impressively, when a high CAL concentration of 5 mmol in water was used, a high CAL conversion of 97.9% with a high COL selectivity of 90.5% can still be attained (Table S4). The reusability is an important catalyst performance indicator and was therefore investigated (Figure 2e). The well-maintained catalytic performance after four-consecutive runs demonstrate a high stability and reusability of Fe_{0.5}Co@NC. This can be attributed to the superior structural stability of Fe_{0.5}Co@NC as evidenced by the almost unchanged structure, morphology, crystal phase and chemical forms of the reused Fe_{0.5}Co@NC (Figures S5-7).

The performance of a alloyed catalyst can be strongly influenced by its alloy composition.^[36] For comparative purpose, the pure Co and Fe NPs (denoted as Co@NC and Fe@NC), and Fe_xCo@NC with different Fe/Co molar ratios ($x = 0.3, 0.7$ and 1.0, Table S1) were synthesised. As shown in Figures S2 and 8, these catalysts possess similar shape and morphology as that of Fe_{0.5}Co@NC. However, the average alloyed NPs sizes are found to increase with the increased Fe content. Their corresponding HRTEM images (Figures S3 and 9) and XRD

patterns (Figures S10) confirm the formation of Fe-Co alloys, which are coincided with the phase diagram of Fe-Co (Figure S11). The XPS survey spectra (Figure S4) and the high resolution Fe 2p and Co 2p spectra (Figure S12) further confirm the formation of Fe-Co alloys. The obviously shifted Fe and Co binding energies in Figure S12 indicate the altered electronic structures for both Fe and Co in the alloys.^[23,37] The Raman spectra display a pair of peaks at 1340 and 1600 cm^{-1} (Figure S13), corresponding to the disordered carbon (D-band) and graphitic carbon (G-band).^[38] Noticeably, the BET surface areas are found to decrease with increased Fe contents (Table S1 and Figure S14).

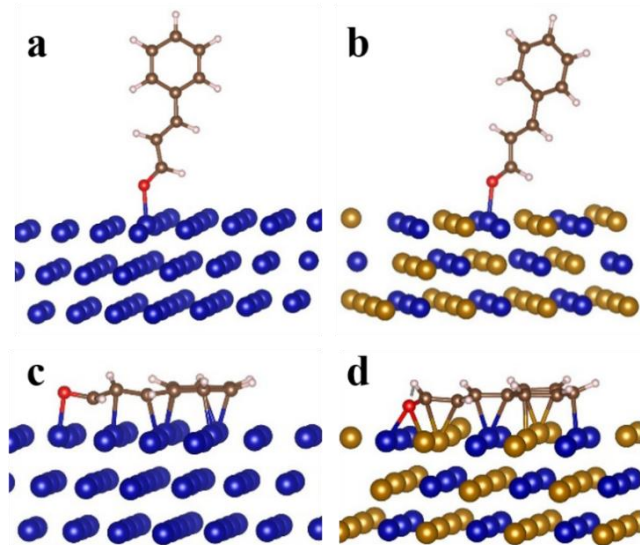


Figure 3. DFT Optimized geometries for CAL adsorbed on the catalyst surfaces with vertical and parallel configurations. (a) Co (111) and (b) Fe-Co (110) with vertical configurations; (c) Co (111) and (d) Fe-Co (110) with parallel configurations. Orange, blue, brown, red, and white spheres represent iron, cobalt, carbon, oxygen and hydrogen atoms, respectively.

To identify the role of Fe and Co, the performance of Fe@NC, Co@NC and Fe_xCo@NC were performed (Figure 2f and Table S5). Fe@NC exhibits poor catalytic activity with 8.9% CAL conversion efficiency, but a relatively high COL selectivity (58.7%), indicating that the Fe catalysed hydrogenation on C=O is more favoured. In strong contrast, Co@NC possess high catalytic activity to achieve almost 100% conversion, probably due to the presence of Co-N_x active sites, which has been demonstrated by our previous study,^[28] however, very poor COL selectivity (< 1%), indicating an indiscriminate hydrogenation of C=C and the C=O by Co. As expected, for the alloyed catalysts, an increase in the Fe content leads to a decreased CAL conversion efficiency. Interestingly, the COL selectivity of Fe_xCo@NC is increased when Fe/Co molar ratios are increased to 0.5, then decreased with further increased Fe/Co molar ratios, indicating an alloying induced synergistic effect due to the electronic structural changes of alloyed Fe and Co as evidenced by the shifted Fe 2p and Co 2p peaks shown in Figure S12. To be specific, the Co⁰ peak shifted from 779.3 eV in Co@NC to 779.0 eV in Fe_{0.5}Co@NC, while the Fe⁰ peak shifted from 707.1 eV in Fe@NC to 707.4 eV in Fe_{0.5}Co@NC, which are resulted from an increased electron cloud density of Co by alloying with Fe species. These suggest that CAL preferred to adsorb on Fe-Co alloy *via* C=O bond rather than C=C because the higher

electron cloud density of Co tends to attack the electrophilic C=O rather than the nucleophilic C=C.^[14,39-41]

The preferred adsorption and activation of CAL at the alloyed metallic sites could be responsible for the high performance achieved by the alloyed catalysts.^[14,39] To verify this hypothesis, H₂ temperature-programmed desorption (H₂-TPD) on Co@NC and Fe_{0.5}Co@NC was conducted. As shown in Figure S15a, the desorption peak of Fe_{0.5}Co@NC is 65 °C higher than that of Co@NC, confirming a change of active sites from Co to Fe-Co sites.^[40,42] The preferred adsorption of CAL on the Fe-Co alloyed surface can be directly evidenced by the Fourier transform infrared (FT-IR) spectra shown in Figure S15b, where, the adsorbed CAL on Fe_{0.5}Co@NC is clearly visible.

The density function theory (DFT) calculations were performed to unveil the critical role of Fe-Co alloy for the improved COL selectivity. Based on the experimentally measured structural characteristics of Fe_xCo@NC, the (111) plane of Co and the (110) plane of Fe-Co alloy were chosen for the DFT calculations. **Figure 3** shows the most stable CAL adsorption configurations with vertical and parallel adsorptions on the (111) plane of Co and (110) plane of Fe-Co alloy. For Co (111) and Fe-Co (110), the calculated adsorption energy (E_{ad}) with vertical configurations are -0.54 and -7.82 eV, respectively (Figure 3a-b). However, with parallel configurations, E_{ad} values are -1.42 and -7.18 eV, respectively (Figure 3c-d), which mean that CAL prefers to adsorb on the (110) plane of the Fe-Co alloy and (111) plane of the metallic Co with vertical and parallel configurations, respectively. These DFT results are well consistent with the obtained experimental results. The preference of vertical configuration with Fe-Co alloy catalyst imply that the high COL selectivity achieved by Fe_{0.5}Co@NC is likely due to the adsorption of CAL selectively through C=O. Figure S16 shows the deformation charge density of CAL adsorption on Fe-Co alloyed surface with the vertical configuration. The transferred charge from the Fe-Co alloy surface to the O atom in C=O of CAL is 0.26 e⁻ more than that from the pure Co surface, for which, the most of the transferred electrons are contributed by the alloyed Fe atoms. This suggests that the C=O in CAL is activated through losing electrons from its O atom to the alloyed Fe atoms. Besides, the C=O in CAL is activated through losing electrons, which can be reflected by the increased C=O bond lengths from 1.230 to 1.264 and 1.268 Å for Co and Fe-Co activated CAL, respectively.

In summary, an alloying strategy is proposed and experimentally validated to dramatically enhance the performance of Fe-Co bimetallic catalysts toward the SH of CAL to COL in pure water medium. The alloyed catalyst with the optimal Fe/Co ratio of 0.5 can achieve an extraordinary COL selectivity of 91.7% at a 95.1% CAL conversion efficiency. The obtained results unveil that the CAL conversion efficiency and COL selectivity can be readily tuned by altering the Fe and Co molar ratio, while the synergism of the alloyed Fe-Co is key to concurrently achieve high COL selectivity and CAL conversion efficiency. The demonstrated transition-metals alloying strategy in this work could be adaptable to concurrently improve the conversion efficiency and selectivity of other hydrogenation reactions.

Acknowledgements

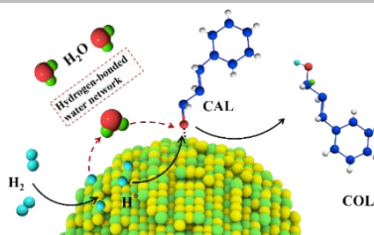
This work was financially supported by the Natural Science Foundation of China (Grant No. 51871209 and 51902311), the Postdoctoral Science Foundation of China (Grant No. 2019M652223).

Keywords: Fe-Co nanoalloys • Metal-organic frameworks • Selective hydrogenation • Cinnamaldehyde • H₂O solvent

- [1] M. Zhao, K. Yuan, Y. Wang, G. Li, J. Guo, L. Gu, W. Hu, H. Zhao, Z. Tang, *Nature* **2016**, 539, 76-80.
- [2] C. H. Hao, X. N. Guo, Y. T. Pan, S. Chen, Z. F. Jiao, H. Yang, X. Y. Guo, *J. Am. Chem. Soc.* **2016**, 138, 9361-9364.
- [3] R. G. Rao, R. Blume, T. W. Hansen, E. Fuentes, K. Dreyer, S. Moldovan, O. Ersen, D. D. Hibbitts, Y. J. Chabal, R. Schlogl, J. P. Tessonnier, *Nat Commun.* **2017**, 8, 340-350.
- [4] C. M. Cova, A. Zuliani, M. J. Munoz-Batista, R. Luque, *Green Chem.* **2019**, 21, 4712-4722.
- [5] K. Yuan, T. Song, D. Wang, X. Zhang, X. Gao, Y. Zou, H. Dong, Z. Tang, W. Hu, *Angew. Chem. Int. Ed.* **2018**, 57, 5708-5713.
- [6] Y. Dai, X. Gao, X. Chu, C. Jiang, Y. Yao, Z. Guo, C. Zhou, C. Wang, H. Wang, Y. Yang, *J. Catal.* **2018**, 364, 192-203.
- [7] M. Butt, X. Feng, Y. Yamamoto, A. I. Almansour, N. Arumugam, R. S. Kumar, M. Bao, *Asian J. Org. Chem.* **2017**, 6, 867-872.
- [8] S. Fujiwara, N. Takanashi, R. Nishiyabu, Y. Kubo, *Green Chem.* **2014**, 16, 3230-3236.
- [9] B. Wu, H. Huang, J. Yang, N. Zheng, G. Fu, *Angew. Chem. Int. Ed.* **2012**, 51, 3440-3443.
- [10] Y. Bonita, V. Jain, F. Geng, T. P. O'connell, N. X. Ramos, N. Rai, J. C. Hicks, *Appl. Catal. B.* **2020**, 277, 119272-119283.
- [11] R. Gao, L. Pan, H. Wang, Y. Yao, X. Zhang, L. Wang, J. J. Zou, *Adv. Sci.* **2019**, 6, 1900054.
- [12] Y. Zhu, H. Qian, B. A. Drake, R. Jin, *Angew. Chem. Int. Ed.* **2010**, 49, 1295-1298.
- [13] H. Liu, L. Chang, L. Chen, Y. Li, *ChemCatChem* **2016**, 8, 946-951.
- [14] H. Wang, S. Bai, Y. Pi, Q. Shao, Y. Tan, X. Huang, *ACS Catal.* **2018**, 8, 154-159.
- [15] N. Mahata, F. Gonçalves, M. F. R. Pereira, J. L. Figueiredo, *Appl. Catal. A.* **2008**, 339, 159-168.
- [16] G. Wang, H. Xin, Q. Wang, P. Wu, X. Li, *J. Catal.* **2020**, 382, 1-12.
- [17] P. Maity, S. Yamazoe, T. Tsukuda, *ACS Catal.* **2013**, 3, 182-185.
- [18] B. Y. Xia, Y. Yan, N. Li, H. B. Wu, X. W. Lou, X. Wang, *Nat. Energy* **2016**, 1, 15006-15014.
- [19] S. Liu, Z. Wang, S. Zhou, F. Yu, M. Yu, C. Y. Chiang, W. Zhou, J. Zhao, J. Qiu, *Adv. Mater.* **2017**, 29, 1700874.
- [20] J. Meng, C. Niu, L. Xu, J. Li, X. Liu, X. Wang, Y. Wu, X. Xu, W. Chen, Q. Li, Z. Zhu, D. Zhao, L. Mai, *J. Am. Chem. Soc.* **2017**, 139, 8212-8221.
- [21] C. Zhao, X. Dai, T. Yao, W. Chen, X. Wang, J. Wang, J. Yang, S. Wei, Y. Wu, Y. Li, *J. Am. Chem. Soc.* **2017**, 139, 8078-8081.
- [22] Y. Xiong, Y. Yang, F. J. Disalvo, H. D. Abruna, *J. Am. Chem. Soc.* **2019**, 141, 10744-10750.
- [23] C.-Y. Su, H. Cheng, W. Li, Z.-Q. Liu, N. Li, Z. Hou, F.-Q. Bai, H.-X. Zhang, T.-Y. Ma, *Adv. Energy Mater.* **2017**, 7, 1602420.
- [24] H. Xin, Y. Xue, W. Zhang, P. Wu, X. Li, *J. Catal.* **2019**, 380, 254-265.
- [25] Jiang, M.; Fu, C.; Cheng, R.; Zhang, W.; Liu, T.; Wang, R.; Zhang, J.; Sun, B., *Adv. Sci.* **2020**, DOI: 10.1002/adv.202000747.
- [26] S. Sultan, J. N. Tiwari, J.-H. Jang, A. M. Harzandi, F. Salehnia, S. J. Yoo, K. S. Kim, *Adv. Energy Mater.* **2018**, 8, 1801002.
- [27] W. Zhang, X. Jiang, X. Wang, Y. V. Kaneti, Y. Chen, J. Liu, J. S. Jiang, Y. Yamauchi, M. Hu, *Angew. Chem. Int. Ed.* **2017**, 56, 8435-8440.
- [28] Y. He, S. Hwang, D. A. Cullen, M. A. Uddin, L. Langhorst, B. Li, S. Karakalos, A. J. Kropf, E. C. Wegener, J. Sokolowski, M. Chen, D. Myers, D. Su, K. L. More, G. Wang, S. Litster, G. Wu, *Energy Environ. Sci.* **2019**, 12, 250-260.
- [29] W. Gong, Y. Lin, C. Chen, M. Al-Mamun, H. S. Lu, G. Wang, H. Zhang, H. Zhao, *Adv. Mater.* **2019**, 31, 1808341.
- [30] Z. Wang, Y. Dong, H. Li, Z. Zhao, H. B. Wu, C. Hao, S. Liu, J. Qiu, X. W. Lou, *Nat. Commun.* **2014**, 5, 5002-5010.
- [31] W. Gong, M. Han, C. Chen, Y. Lin, G. Wang, H. Zhang, H. Zhao, *ChemCatChem* **2020**, 12, 1019-1024.
- [32] Y. Deng, R. Gao, L. Lin, T. Liu, X. D. Wen, S. Wang, D. Ma, *J. Am. Chem. Soc.* **2018**, 140, 14481-14489.
- [33] W. Gong, C. Chen, Y. Zhang, H. Zhou, H. Wang, H. Zhang, Y. Zhang, G. Wang, H. Zhao, *ACS Sustainable Chem. Eng.* **2017**, 5, 2172-2180.
- [34] W. Yang, X. Liu, X. Yue, J. Jia, S. Guo, *J. Am. Chem. Soc.* **2015**, 137, 1436-1440.
- [35] L. He, F. Weniger, H. Neumann, M. Beller, *Angew. Chem. Int. Ed.* **2016**, 55, 12582-12596.
- [36] H. Guo, H. Li, K. Jarvis, H. Wan, P. Kunal, S. G. Dunning, Y. Liu, G. Henkelman, S. M. Humphrey, *ACS Catal.* **2018**, 8, 11386-11397.
- [37] X. Zhu, T. Jin, C. Tian, C. Lu, X. Liu, M. Zeng, X. Zhuang, S. Yang, L. He, H. Liu, S. Dai, *Adv. Mater.* **2017**, 29, 1704091.
- [38] Y. Li, B. Jia, Y. Fan, K. Zhu, G. Li, C.-Y. Su, *Adv. Energy Mater.* **2018**, 8, 1702048.
- [39] C. Yang, S. Bai, Y. Feng, X. Huang, *ChemCatChem* **2019**, 11, 2265-2269.
- [40] Y. S. Yang, D. M. Rao, Y. D. Chen, S. Y. Dong, B. Wang, X. Zhang, M. Wei, *ACS Catal.* **2018**, 8, 11749-11760.
- [41] Hui, T.; Miao, C.; Feng, J.; Liu, Y.; Wang, Q.; Wang, Y.; Li, D., *J. Catal.* **2020**, 389, 229-240.
- [42] T. Ishihara, N. Horiiuchi, T. Inoue, K. Eguchi, Y. Takika, H. Arai, *J. Catal.* **1992**, 136, 232-241.

COMMUNICATION

A bimetallic Fe-Co alloying strategy is innovatively utilized to concurrently enhance the selectivity and conversion efficiency for selective hydrogenation of cinnamaldehyde to cinnamyl alcohol in water. A Fe-Co alloy catalyst with a Fe/Co molar ratio of 0.5 achieves an exceptional selectivity of 91.7% at 95.1% conversion.



Y. Lv[†], M. Han[†], W. Gong^{*}, D. Wang, C. Chen, G. Wang, H. Zhang, H. Zhao^{*}

Page No. – Page No.

**Fe-Co Alloyed Nanoparticles
Catalysed Efficient Hydrogenation of
Cinnamaldehyde to Cinnamyl Alcohol
in Water**